Check for updates

Development of a Low-Turbulence Transverse-Gust Generator in a Wind Tunnel

David A. Olson,* Ahmed M. Naguib,† and Manoochehr M. Koochesfahani‡
Michigan State University, East Lansing, Michigan 48824

https://doi.org/10.2514/1.J059962

This work demonstrates the viability of a novel transverse-gust generator that is capable of producing a controllable time-varying gust without increasing the turbulence level within a large region of the flow facility. The new gust-generator concept is based on a vortex-generator array (VGA) along one of the walls of a facility's test section at a given streamwise location. Using such a device, a steplike gust and a sinusoidal gust with amplitudes of 5.7% of freestream velocity are demonstrated in a wind tunnel. The sinusoidal gust produces practically pure-harmonic oscillation in the freestream's direction of ±3.25 deg at a frequency of 2 Hz for a freestream speed of 10 m/s. A simplified vortex-array model is shown to be a viable tool for the design of the new gust generator. This study is focused on demonstrating the concept of the VGA gust generator while leaving the generator's design optimization and the exploration of the limits of the gust strength and uniformity to future work.

Downloaded by MICHIGAN STATE UNIVERSITY on January 21, 2021 | http://arc.aiaa.org | DOI: 10.2514/1.J059962

Nomenclature

AR	=	vortex-generator aspect ratio
b_{VG}	=	vortex-generator span
c_{VG}	=	vortex-generator chord
H	=	height of test section
R	=	vortex core radius
Re_c	=	vortex-generator chord Reynolds number; $U_\infty c_{\mathrm{VG}}/\nu$
r	=	radial coordinate from the center of a vortex
U_∞	=	freestream velocity
u	=	streamwise flow velocity component
VG	=	vortex generator
v	=	transverse flow velocity component
W	=	width of test section
w	=	spanwise flow velocity component
X	=	streamwise coordinate
Y	=	transverse coordinate
Z	=	spanwise coordinate
α_{VG}	=	angle of attack of the vortex generators
Γ	=	circulation
Γ_o	=	vortex circulation
Δ_{VG}	=	interspacing of the vortex generators
ν	=	kinematic viscosity
$\omega_{\max}$	=	vorticity at the core center of a vortex

I. Introduction

A STEADY uniform freestream condition is typically employed when evaluating the aerodynamic performance of airfoils, wings, aircraft, and aero- and hydrodynamic bodies in general. However, there are numerous situations when an aerodynamic body must perform in a more complex flow environment. While the interaction of, for example, an airfoil with a transient event (such as a streamwise gust) has long been considered, transverse gusts (see Fig. 1 for illustration) have been addressed in fewer studies because they are harder to create experimentally (e.g., see discussions in Refs. [1,2]). Recent interest in the performance of low-Reynolds-number unmanned aerial vehicles in the highly turbulent urban environment has energized research efforts focused on airfoil aerodynamics in the presence of high-amplitude transverse gusts; e.g., Refs. [1–4]. In Refs. [1,2], a cross-stream water jet in a tow tank is used to create a *steady* gust having sine-squared and top-hat velocity profiles, respectively. In this case, the *unsteady* strong-gust encounter is produced by traversing the airfoil across the steady cross-stream jet at a velocity comparable to that of the gust. A similar approach, allowing strong-gust generation (but while keeping the airfoil stationary), is reported in Refs. [3,4], where a blower assembly is employed to create a transient *steplike* transverse gust in a wind tunnel operating at a low freestream speed (1.5 m/s). Even though both of the aforementioned approaches create strong transverse gusts [with velocity up to the same order as the freestream velocity; i.e., $\mathcal{O}(1)$ gust ratio], they have distinct limitations: the first approach [1,2] produces large turbulent fluctuation about the mean gust velocity (10–20% of freestream), and the second [3,4] creates a spatially nonuniform gust within the test section while also increasing the freestream turbulence. Additionally, tow-tank approaches are not easily adaptable to produce sustained periodic gust encounters.

From broader perspective, very strong gusts with $\mathcal{O}(1)$ gust ratio (or equivalently freestream direction variation of 45 deg) are not typical for most aviation applications. While the limitations imposed by turbulence and the reduced versatility of gust generation need to be tolerated to produce these strong gusts, it is generally desirable to avoid these limitations to enable independent and flexible generation of freestream complexities. Studies aiming to produce transverse gusts while avoiding/minimizing the addition of turbulence into the flow have predominantly focused on two different approaches that are based on a common principle, although their mode of implementation is fundamentally different. The common principle is that of producing the gust from the *far-field* disturbance of vortices. As seen in Fig. 2, the two approaches use a pair of oscillating airfoils for generation of the vortices. In the first approach (Fig. 2a), which is the one most extensively used [5–7], the two two-dimensional (2-D) airfoils are placed upstream of the test model, with their axes parallel to that of the test airfoil. The generator airfoils are positioned near the test-section sidewalls, leaving the central portion undisturbed by turbulence from the wake of the airfoils. The von Kármán vortex street of counter-rotating vortex pairs in the wake of the oscillating airfoils induces both streamwise and transverse-gust velocities (u and v, respectively) in the central portion of the test section, where the test airfoil is placed. When the two airfoils oscillate in phase with the same amplitude, the v disturbance on the center plane of the tunnel is twice that produced by one of the airfoils, whereas the u disturbance cancels out.

Presented as Paper 2020-2041 at the AIAA Scitech 2020 Forum, Orlando, FL, January 6–10, 2020.; received 6 July 2020; revision received 5 October 2020; accepted for publication 21 October 2020; published online 30 November 2020. Copyright © 2020 by the authors. Published by the American Institute of Aeronautics and Astronautics, Inc., with permission. All requests for copying and permission to reprint should be submitted to CCC at www.copyright.com; employ the eISSN 1533-385X to initiate your request. See also AIAA Rights and Permissions www.aiaa.org/randp.

*Research Associate, Mechanical Engineering, 1449 Engineering Research Ct. A109. Member AIAA.

†Professor, Mechanical Engineering, 1449 Engineering Research Ct. C128. Associate Fellow AIAA.

‡Professor, Mechanical Engineering, 1449 Engineering Research Ct. A131. Associate Fellow AIAA.

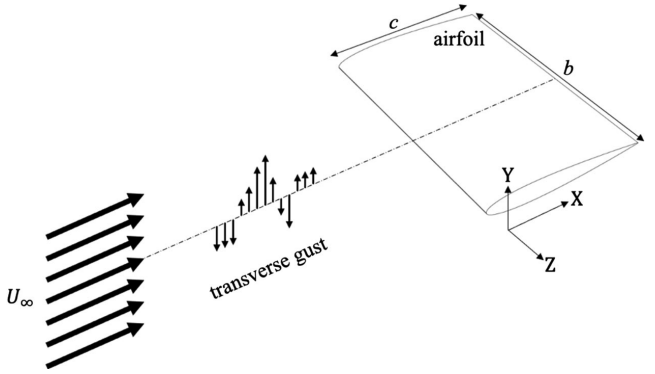

Fig. 1 Illustration of an airfoil exposed to unsteady transverse gust in the Y direction superposed on uniform approach freestream.

The performance of the gust generator in Fig. 2a relies on a tradeoff between gust strength and gust uniformity (in the Y direction). The strength of the induced v fluctuation decays with distance from the centerline of the generator's wake, yet the uniformity improves. For the von Kármán vortex arrangement, the v fluctuation decays relatively quickly with distance from the wake centerline owing to the fact that in the cross-stream far-field, the contribution from one "row" of vortices with a given vorticity sign is approximately equal in magnitude but opposite in direction to that from the other row. In other words, in the far field, the gust is produced by the small difference between the induced velocity of half the wake vortices and that of the other half. Another limitation is that, to maintain an orderly vortex structure of counter-rotating vortex pair per oscillation cycle, the amplitude α_o of the airfoil pitch oscillation must be kept sufficiently small to avoid the formation of leading-edge vortices as well as thickening of the wake. These added complexities would adversely influence the ability to produce controlled harmonic, or near-harmonic, gusts and gust uniformity. This leaves the oscillation frequency as the main parameter to control *both* the strength and the frequency of the gust when good gust uniformity is desired.

Using the arrangement in Fig. 2a [5,6] demonstrates gust ratios (gust-velocity amplitude divided by the freestream velocity) of up to 9.7% for a relatively large pitch oscillation amplitude of $\alpha_o = 10.1$ deg. The transverse uniformity of the gust was not assessed in these studies. Reference [7] reports the generation of gusts with strength up to 1.5% for α_o up to 5 deg. The best uniformity of the gust corresponds to spatial variation with a standard deviation of approximately 20% of the gust-velocity amplitude. Other variations on the gust-generator concept in Fig. 2a employ oscillatory circulation control, instead of airfoil oscillation, to produce the periodic wake vortices. In the example in Ref. [8], a pair of air jets injected near the trailing edge produces the oscillation, resulting in transverse gusts with appreciable strengths of almost 16%. However, documentation of gust uniformity at lower strength of 6% shows significant variation in the gust strength over the cross section of the wind tunnel. Another study [9] employed a rotating slotted cylinder at the trailing edge of each of the stationary airfoils to implement unsteady circulation control. Gust ratios of up to 3% were achieved, and gust uniformity was documented only along a vertical line and a horizontal line centered on the test-section cross section. The authors indicate that the wake of the cylinder imposes a major limitation on the generator's performance.

The second gust-generator arrangement, shown in Fig. 2b, employs short-span airfoils/vanes placed directly upstream of the test model to produce the gust. The short span of the airfoils ensures that wake turbulence is confined near the sidewalls, away from the test model. For this arrangement, the transverse gust is induced by the *tip vortices* of the short-span airfoils [or vortex generators (VGs)]. The amplitude of the gust is controlled by the amplitude of the VG's pitch oscillation, and the frequency of the gust is controlled by the oscillation frequency. The use of this approach to study gust loading on a fighter-aircraft model is reported in Ref. [10]. In this study, gusts with strengths up to 2.4% at frequencies up to 20 Hz are demonstrated. Limited characterization of the gust uniformity showed reasonable uniformity along the tunnel centerline. However, significant variations are observed off centerline in both Y and Z directions. In addition to the limited uniformity, the arrangement shown in Fig 2b also constrains the span of the test airfoil from extending across the

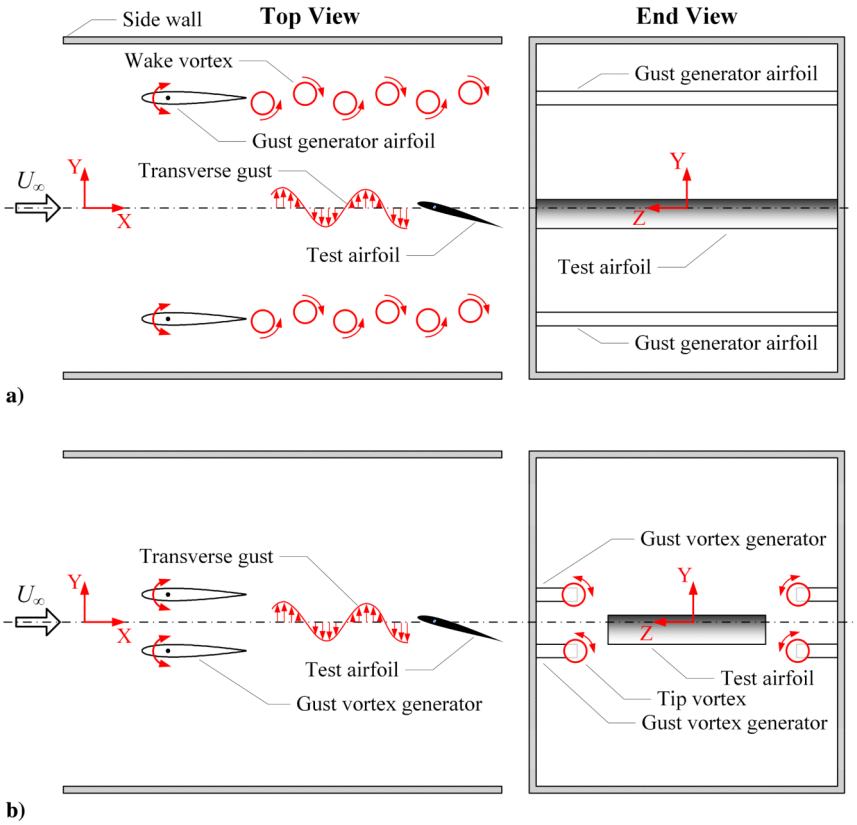

Fig. 2 Illustration of two concepts of transverse-gust generators.

Downloaded by MICHIGAN STATE UNIVERSITY on January 21, 2021 | http://arc.aiaa.org | DOI: 10.2514/1.J059962

Downloaded by MICHIGAN STATE UNIVERSITY on January 21, 2021 | http://arc.aiaa.org | DOI: 10.2514/1.J059962

full width of the tunnel to avoid turbulence from the wake of the generator's airfoils. The latter limitation can be overcome using a sting mount or shrouded sidewall support. On the other hand, since the approach is not limited to small α_o as the one discussed earlier in this paper, the tip-vortex-based approach seems to be more flexible in controlling the amplitude and the frequency of the gust independently. Moreover, unlike the concept in Fig. 2a, where the gust velocity induced by half the vortices opposes that from the other half, the two tip vortices from the vortex generators in Fig. 2b induce gust velocities in the same direction when phased properly.

The present study seeks to evaluate a novel transverse-gust-generation device that introduces unsteady gusts with good uniformity into a flow facility while maintaining low turbulence fluctuation levels, and with a high degree of controllability in terms of the magnitude, the duration, and the time history of the gust. The device is based on extending the method illustrated in Fig. 2b by using an *array* of tip-vortex generators, *mounted along the full width* of the tunnel, instead of only two vortex generators. Given the constructive superposition of the effect of each vortex generator, the array implementation holds the potential for achieving stronger, more uniform gusts, with an added degree of freedom in controlling the gust strength by the interspacing of the vortex generators. Other benefits, along with limitations, as well as implementation and characterization of this vortex-generator array (VGA) concept are discussed in the remainder of the paper.

II. Gust-Generator Design and Model

The design of the transverse-gust generator consists of an array of vortex generators mounted on one wall of the test section, as shown in Fig. 3. Each vortex generator is a NACA 0012 airfoil whose tip is a body of revolution. A rounded wing tip is selected to reduce the strength of secondary vortices produced from the interaction of the main vortex with the VG surface while also expediting the vortex reaching the axisymmetric flow condition, as discussed in Ref. [11]. A slider (shown in gold in the bottom of Fig. 4) links all of the vortex

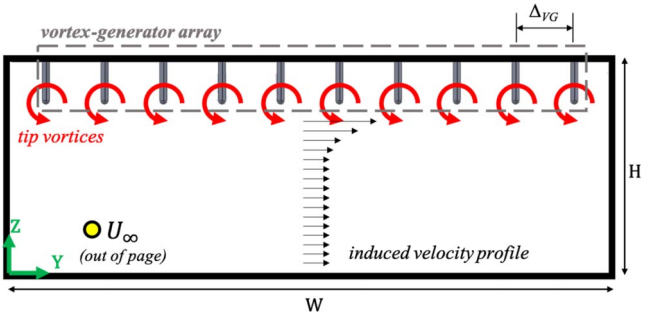

Fig. 3 Cross-sectional (end) view of the test section where the freestream is out of the page. Red arrows indicate vortex sign. For the present experiments, H = 216 mm and W = 610 mm.

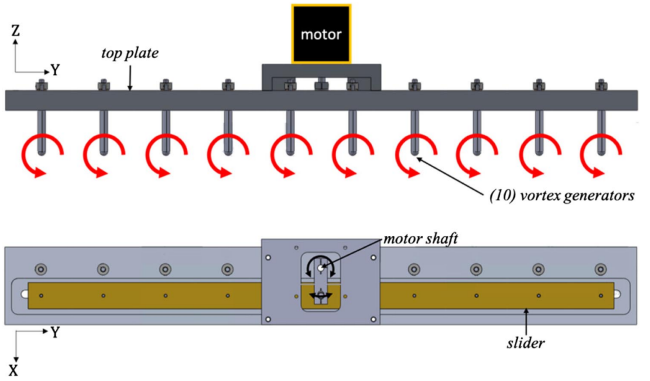

Fig. 4 Two-view drawing of the gust generator. End view (top) of the vortex-generator array. Top view (bottom) does not include the motor to show the motor linkage to the slider (gold). Red arrows indicate vortex sign.

generators together such that they can be actuated by a centralized pitch motor. The flow is minimally disturbed when the VGs are at a zero angle of attack; however, when the VGs are pitched to a nonzero angle of attack, a tip vortex forms from each VG (as indicated by the red arrows in Figs. 3 and 4). The induced velocity field from this array of streamwise vortices constitutes the transverse gust in the central (core) region of the test section. For a given array configuration (the VGs airfoil's shape, chord and span, and interspacing), the angle of attack of the VGs is the mechanism to change the strength of the tip vortex, and therefore the strength of the gust. In addition, by dynamically changing the angle of attack, it is possible to control the duration and the waveform of the gust.

While significant velocity fluctuation is expected to possibly occur in the core of each tip vortex, the induced flow away from the center of the vortex cores should remain reasonably steady with little fluctuation other than that from the baseline freestream turbulence and the imposed gust unsteadiness. This yields a large portion of the test section where a transverse gust can be introduced into the flow facility without impacting the freestream turbulence level.

The vortices produced by the VGA are modeled through superposition of the induced velocities of their tip vortices (see Ref. [12] for details of a similar model applied to the wake of an oscillating airfoil). For simplicity, each tip vortex is modeled as an infinite vortex tube with a Gaussian vorticity distribution of the form

$$\omega(r) = \omega_{\max} e^{-(r/R)^2} \tag{1}$$

where $\omega_{\max}$ is the vorticity at the vortex core center, r is the radial coordinate measured from the vortex core center, and R is the vortex core radius. The corresponding circulation profile is given by

$$\Gamma(r) = \Gamma_o \left[1 - e^{-(r/R)^2}\right] \tag{2}$$

where Γ_o is the vortex circulation in the limit $r \to \infty$, and it can be shown that

$$\Gamma_o = \pi R^2 \omega_{\max} \tag{3}$$

In the preceding equations, the values for Γ_o and $\omega_{\max}$ are set using the semiempirical models of Wendt, which connect these vortex parameters to the airfoil's chord, aspect ratio, angle of attack, and the ratio of the airfoil's span to boundary-layer thickness [13–17]. Subsequently, Eq. (3) is used to compute R. The core centers of the vortices are placed at the same Y locations as the vortex generators, 5% inboard of the VG's tip.

The effect of *all* vortices, including their mirror images with respect to all of the walls of the test section, is accounted for using the Biot–Savart law. Twenty of the infinite layers of image vortices are included in model for the design calculations. The effect of additional layers is checked to be negligibly small. Furthermore, the vortex pattern is assumed to be 2-D (i.e., the model excludes the streamwise evolution of the individual vortices), and the vortex pattern development via intervortex interactions is neglected. The viscous boundary layer on the walls is also excluded in the calculation.

An initial parametric study was conducted using the aforementioned model to consider the effect of the aspect ratio, the chord length, the transverse spacing, and the number of the vortex generators. In Figs. 5a, 5c, and 5e, color contour maps of the transverse (gust) velocity v are shown for two, four, and eight vortex generators, whose chord is $c_{\mathrm{VG}} = 80$ mm, aspect ratio is $AR = 0.73$, transverse spacing is $\Delta_{\mathrm{VG}} = 0.75 c_{\mathrm{VG}}$, and angle of attack is $\alpha_{\mathrm{VG}} = 16$ deg. Transverse-velocity profiles versus Y/W, extracted at Z/H = 0.05 and 0.5, are shown in Fig. 5g. Figure 5h shows the transverse-velocity profiles versus Z/H at the center of the test section (Y/W = 0.5). It is observed that as the number of vortex generators increases, the transverse (Y) and spanwise (Z) extent of a nominally uniform-gust-velocity region increases, and the magnitude of the induced velocity increases with an increasing number of vortex generators. Figure 5h shows that the increase in the transverse velocity below Z/H = 0.5, at the center of the array, is smaller between four and

Downloaded by MICHIGAN STATE UNIVERSITY on January 21, 2021 | http://arc.aiaa.org | DOI: 10.2514/1.J059962

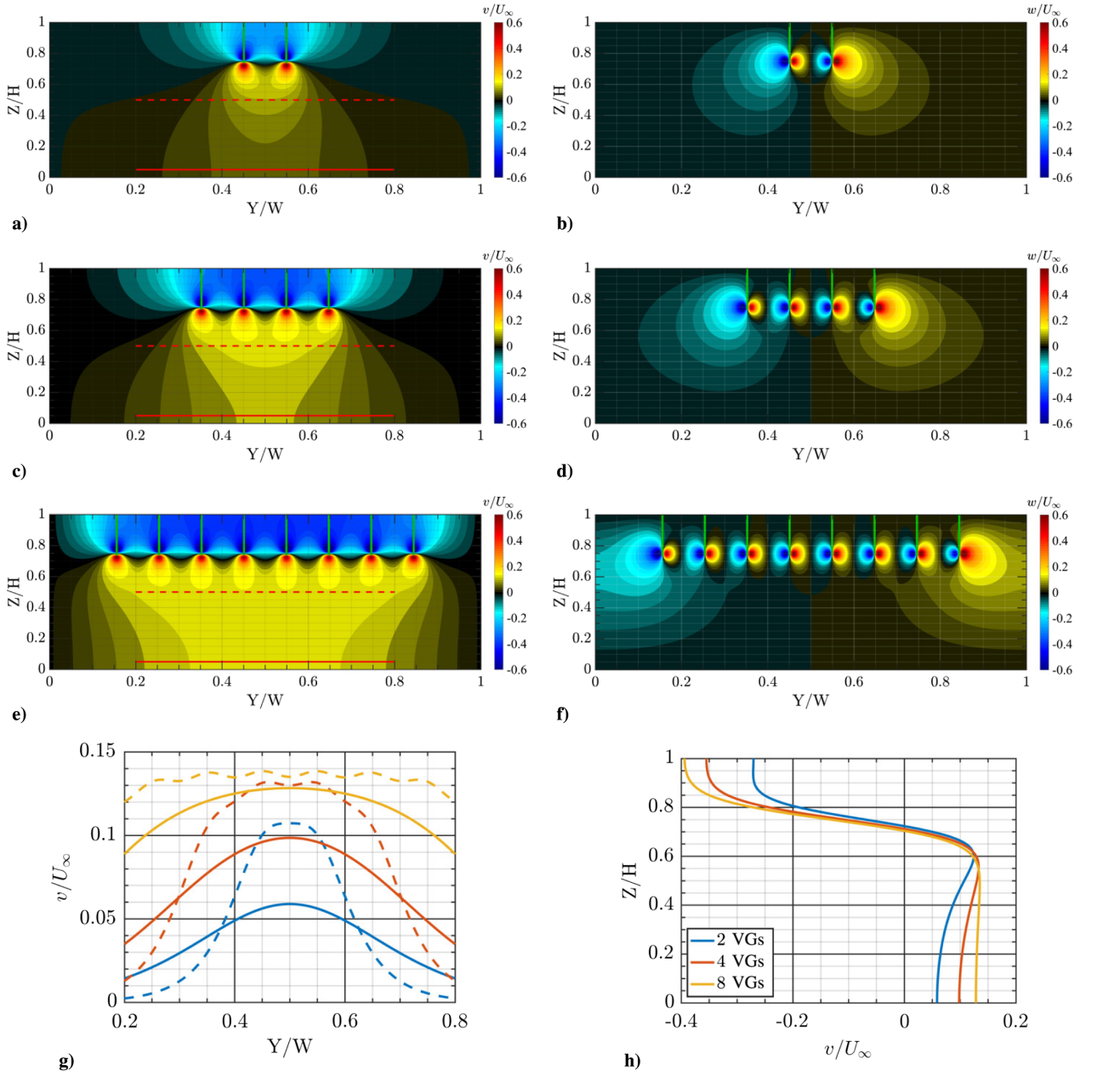

Fig. 5 Results of vortex-array model: a,c,e) flooded contours of transverse v-velocity and b,d,f) spanwise w-velocity for two (Figs. 5a–5b), four (Figs. 5c–5d), and eight (Figs. 5e–5f) vortex generators. Figure 5g shows profiles of transverse v-velocity extracted at $Z/H = 0.5$ (broken line) and $Z/H = 0.05$ (solid line), with color indicating number of vortex generators as given in legend of Fig. 5h. Figure 5h shows transverse v-velocity profiles extracted at $Y/W = 0.5$.

eight VGs compared to the initial increase from two to four VGs. Generally, beyond a certain number of generators, increasing the number of VGs primarily improves the gust uniformity in the test section (in both the Y and Z directions) with little change in the gust strength. Figure 5g is particularly instructive in highlighting one of the key advantages of extending the gust generator's concept from that using a pair of vortex generators in Fig. 2b to a large-array implementation. The significant deterioration in gust strength and uniformity is evident when using only two VGs.

Another significant point to assess regarding the VGA performance is whether the array introduces significant parasitic lateral (Z) velocity w. This point can be examined by inspection of Figs. 5b, 5d, and 5f, where w distribution over the test-section flow area is depicted via a color contour map when using two, four and eight VGs. Overall, it is evident that the w disturbance produced by the VGs remains confined to the vicinity of the VGs, leaving a good-sized test area with $w \approx 0$ in the core of the test section, where a significant v disturbance also exists. With a pair of vortex generators, the available test area is visibly smaller than that for the larger number of VGs. As the number of VGs increases, the regions with significant w disturbance are displaced to the ends of the array in the Y direction near the facility sidewalls while remaining in the local vicinity of the VGs along the Z direction.

Based on the aforementioned analysis and the physical size of the test section, a preliminary design of the VGA is developed and tested in the wind tunnel. Further optimization of this design is carried out experimentally (discussed in Sec. V), leading to a final design consisting of 10 vortex generators with $c_{VG} = 80$ mm, $AR = 0.73$, $\Delta_{VG} = 0.75 c_{VG}$, and $\alpha_{VG} = 16$ deg. A visual representation of the flowfield produced by this design, based on the vortex-array model, is displayed in Fig. 6. The figure depicts the planar velocity vector field superposed onto a color contour map of the out-of-plane vorticity field. The latter highlights the location of the vortex core centers that, as stated previously, are placed 5% inboard of the tips of the VGA for the model calculation. The velocity vectors demonstrate the gust uniformity over a core area of the test section that extends over the domains $0.4 \leq Y/W \leq 0.6$ and $0.05 \leq Z/H \leq 0.5$ (as outlined by

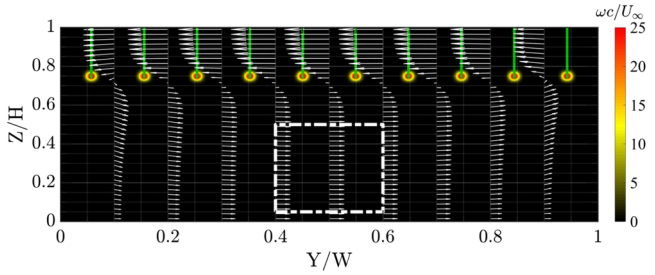

Fig. 6 Flooded contour maps of out-of-plane vorticity in test section for a vortex-generator array consisting of 10 vortex generators (indicated by green lines at top of figure). White broken line encircles nominally uniform-gust domain, and white vectors depict planar velocity vectors formed from gust (v) and spanwise (w) velocity components at selected locations. For reference, the largest vector within the outlined area has a magnitude of 13.6% of U_∞.

the white broken line in Fig. 6). The average transverse v- velocity in this region is 13.3% of U_∞ with a spatial variation [root mean square (RMS)] of less than a 0.2% of U_∞. Nonuniformities in both Y and Z, as well as the presence of a parasitic w velocity, are visible at the ends of the array.

III. Experimental Methods

Experiments are performed in an open-circuit wind tunnel with a test-section cross section of 61×61 cm and a length of 183 cm, located at the Flow Physics and Control Laboratory at Michigan State University. The test section is divided by a false ceiling with the upper section used for instrumentation and the lower section (with a height of H = 21.6 cm) as the primary flow section. A diagram of the test section is shown in Fig. 7, whereas a more complete description of the setup can be found in the work of Hamedani et al. [18].

The flowfield is characterized downstream of the vortex-generator array (gust generator) using an X-wire probe. The hot wires are made from 5-μm-diameter tungsten with a sensing length of 1 mm ($0.0125c_{VG}$). The corresponding sensing volume is approximately 1 mm^3. The probe is oriented to measure the streamwise and cross-stream/transverse (gust) velocity components; u and v, respectively. Each wire is connected to a single channel of a TSI IFA-300 constant temperature anemometer and is operated at an overheat ratio of 0.6. A 1 kHz low-pass filter is applied on board of the anemometer, whereas the output voltage of each wire is acquired at 2 kHz on a National Instruments PCI-6034E 16-bit data acquisition board. The wires are calibrated against a pitot tube, and a cosine-law yaw dependence of the wires is used with the measured wire orientations relative to the test-section walls. The wire magnitude response is fitted to King's law, and the temperature compensation method of Hultmark and Smits [19] is applied to correct for temperature variation within the wind tunnel during measurements, which was typically within 2°C. Measurement uncertainty due to hot-wire calibration drift is within ±2% for the results presented herein.

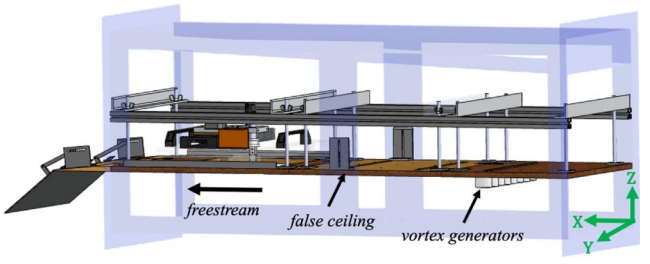

Fig. 7 Drawing of test section with vortex-generator array installed in false ceiling at upstream end of test section (flow is right to left). Coordinate system is aligned such that X indicates streamwise direction, Y indicates transverse (gust) direction, and Z depicts spanwise direction of test airfoil that would be subjected to transverse gust. Corresponding velocity components are u, v, and w in the respective directions.

Measurements are performed over the full width (W = 61 cm) and height (H = 21.6 cm) of the test section at a freestream velocity of $U_\infty = 10$ m/s. This is accomplished by moving the probe using a stepper-motor-controlled 2-D traversing system. Measurement spacing was 5 mm in the Y-direction and 3 mm in the Z-direction, with each measurement consisting of nominally 118×67 points in the Y and Z directions, respectively. At each measurement location, the velocity is sampled for 18 s, during which the VGA is in the "off" configuration for 3 s, followed by actuation of the VGA for 12 s, and then a return to the off configuration. This measurement scheme is sufficient to allow capturing the gust-velocity time series before, during, and following the VGA actuation, after early on/off actuation transients have completely decayed.

The VGA actuations considered are: a steplike maneuver from $\alpha_{VG} = 0$ deg to $\alpha_{VG} = +16$ deg (and its return to 0 deg), and a sinusoidal variation of α_{VG}, with an amplitude of 16 deg and a frequency of 2 Hz. The hot-wire probe outputs are sampled for at least 2.5 s under each steady-state condition, which corresponds to 312 convective times based on the vortex-generator chord length and the freestream velocity. The resulting random uncertainty in mean-velocity measurements is 0.2% of the freestream velocity.

IV. Results

Starting with the initial VGA design based on the vortex-array model, several different VGA arrangements with varying chord, aspect ratio, and spacing were considered experimentally. Results from characterizing several of these configurations for $\alpha_{VG} = 16$ deg are summarized in Fig. 8, where the transverse v-velocity profiles extracted at a height of Z/H = 0.36 are shown across the width of the test section for measurement at 350 mm downstream of the VGA. Testing of $c_{VG} = 60$ mm vortex generators shows that increasing the spacing from $\Delta_{VG} = 0.5c_{VG}$ to $\Delta_{VG} = 1.0c_{VG}$ greatly improves the uniformity of the transverse v-velocity across the test section, but at the expense of a lower-velocity magnitude. This decrease in gust strength with increasing Δ_{VG} is consistent with modeling results (not shown here), which can be physically connected to the decrease in circulation per unit length of the vortex array. The reason for the corresponding increase in gust uniformity cannot be explained using the model. As will be seen later, the biggest nonuniformity is connected to sideways and top/down movement of the vortices near the wall, which increases progressively with downstream distance: an effect that is not captured in the present vortex-array model. A balance between the magnitude of the induced velocity and uniformity is achieved by increasing the chord of the vortex generators to $c_{VG} = 80$ mm and using $\Delta_{VG} = 0.75c_{VG}$, as seen in Fig. 8. The final VGA configuration consists of an array of 10 vortex generators to fit as many VGs as possible within the available width of the test section.

The array of 10 VGs with chord of $c_{VG} = 80$ mm, span of $b_{VG} = 58$ mm (for an aspect ratio of $AR = 0.73$), and Y- spacing of $0.75c_{VG}$ is characterized using measurements conducted at X = 650 mm ($8.13c_{VG}$) downstream of the trailing edge of the VGA (when

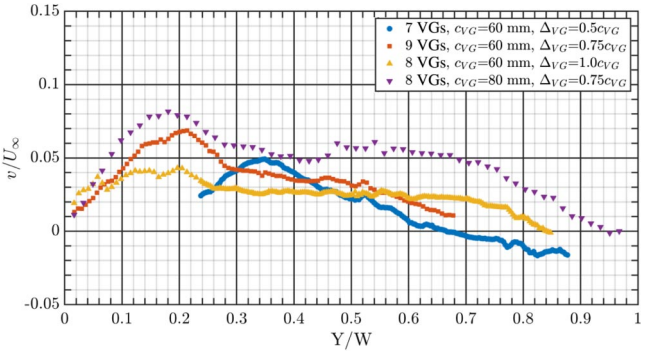

Fig. 8 Mean transverse v-velocity profiles extracted at a Z/H = 0.36 and a streamwise location of 350 mm downstream of the vortex generators for several VGA configurations and $\alpha_{VG} = 6$ deg.

Downloaded by MICHIGAN STATE UNIVERSITY on January 21, 2021 | http://arc.aiaa.org | DOI: 10.2514/1.J059962

Downloaded by MICHIGAN STATE UNIVERSITY on January 21, 2021 | http://arc.aiaa.org | DOI: 10.2514/1.J059962

$\alpha_{VG} = 0$ deg). The VG Reynolds number is $Re_c = 5.2 \times 10^4$, based on $U_\infty = 10$ m/s. Figure 9 shows flooded color contours of the mean transverse v-velocity change between the off and "actuated" steady-state conditions for the steplike actuation from 0 deg to $\alpha_{VG} = +16$ deg. In this plot, the signature of the individual vortices manifests itself in the form of a "dipole" of vertically stacked islands of peak positive and negative v.

Figure 9 is used to analyze two aspects of the gust generator's performance: 1) the behavior of the vortices, and 2) the cross-stream mean flow generated by the static VGs. First, we observe that all except the outboard vortices retain the intended formation of a wall-parallel vortex array. Considering the induced velocity on the outboard vortices, it is expected that the rightmost vortex will move toward the top wall, and the leftmost vortex will move away from the same wall with downstream distance, which is clearly seen in the data. Once the leftmost vortex has moved away far enough, the next inboard vortex is expected to start moving away from the wall as well, which is also observed. On the other hand, the inboard vortices are stabilized by the opposing upwash/downwash effect of their neighboring vortices immediately to the left and to the right, and hence these vortices remain in a well-behaved pattern. In addition to the undesirable up and down movements of the end vortices, the entire vortex array shifts leftward as it convects downstream.

The transverse and the up/down displacement of the vortex array with downstream distance is expected based on the inviscid mutual interactions among the vortices and their wall images. In fact, if the model discussed in Sec. III is developed further to include these interactions, it should reproduce (at least qualitatively) the observed vortex displacements. The results in Fig. 9 show that the horizontal displacement is small enough (slightly more than Δ_{VG}) at the x location of the measurements such that there remains a reasonable number of vortices on both sides of the target test zone in the central portion of the test section. This is another advantage for utilization of an array of VGs versus only two generators, where the lateral motion of only two vortices would significantly offset them laterally relative to the test zone, leading to further decrease in uniformity and/or strength of the gust relative to that produced by a large vortex array.

Considering the steady transverse (v) flow produced in the test-section core region delineated by the broken red line in Fig. 9, the average velocity over this central 20% of the test-section width and 55% of its height is 5.7% of U_∞ with spatial RMS variation over the same domain of less than 0.7% of U_∞ (≈12% of the average gust velocity). More insight into the uniformity of the transverse v-velocity in this region is gained by inspection of Fig. 10, where the velocity profiles along the boundaries of the region are shown. There is more RMS deviation across the upper and lower boundaries (12.0 and 12.1%; Fig. 10a) compared to those along the side boundaries (6.6 and 4.3%; Fig. 10b).

Close inspection of Fig. 10a shows that the nonuniformity in Y is characterized by a side-to-side trend as well as an oscillatory behavior that is more prominent at the top of the core area (close to the VGs) than the bottom. The former variation is connected to the aforementioned up/down translation of the vortices along the test-section sidewalls. As discussed previously, this motion causes vortices at one end of the array to "climb down" the sidewall, whereas vortices on the other end will move in the opposite direction (see Fig. 9). The resulting side-to-side asymmetry in the vortex arrangement is believed to be the main driver of the lateral trend in the gust nonuniformity. The farther downstream the measurement (i.e., test) location is, the larger the vortex movement, and hence the nonuniformity.

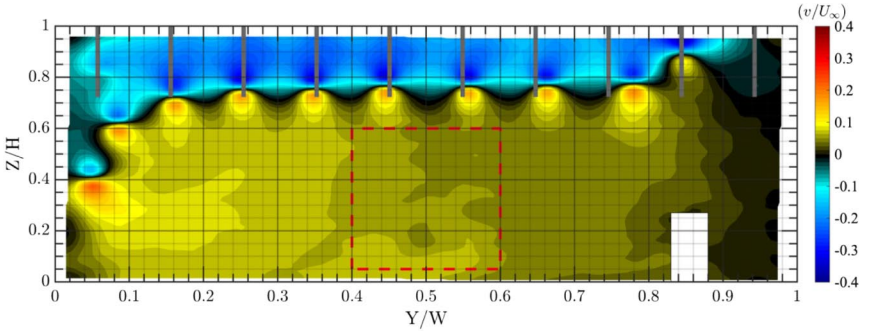

Fig. 9 Measured mean transverse v-velocity change between the baseline condition and steady state after step actuation of the VGA to $\alpha_{VG} = 16$ deg. Results obtained at X = 650 mm ($8.13c_{VG}$) downstream of the vortex-generator array. Data in the region between $0.82 < Y/W < 0.88$ for $Z/H < 0.3$ are excluded since they are immediately downstream of the pitot probe used to measure the freestream velocity.

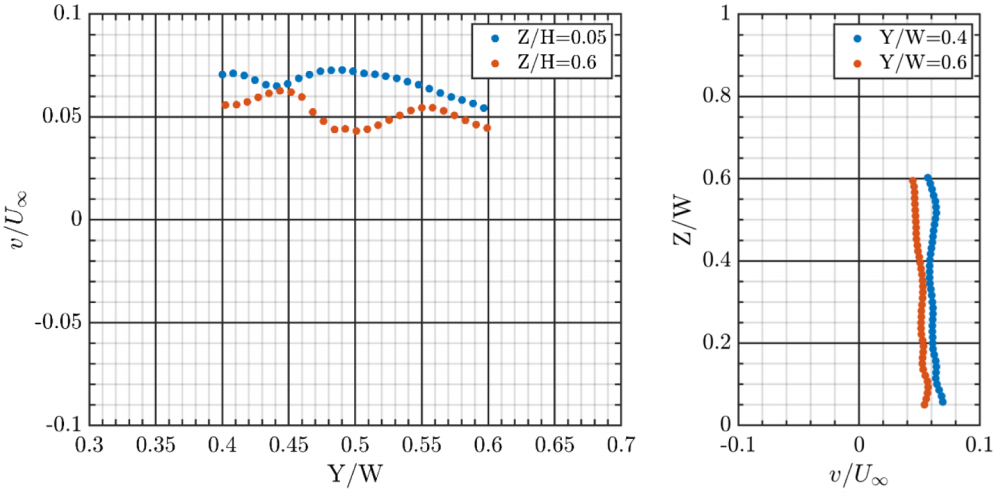

a) Upper/lower boundary profiles **b) Left/right boundary profiles**

Fig. 10 Measured mean transverse v-velocity profiles extracted at a) upper/lower, and b) left/right bounds of the region delineated with a red broken line in Fig. 9. Random uncertainty of the data is less than the symbol size.

Downloaded by MICHIGAN STATE UNIVERSITY on January 21, 2021 | http://arc.aiaa.org | DOI: 10.2514/1.J059962

Thus, one could reduce this nonuniformity by limiting the measurement area to regions closer to the VGA and/or designing a test section with a larger width-to-height ratio so that the asymmetric conditions along the sidewalls are pushed farther away from the test area. To aid in estimating the distance downstream of the VGA over which the gust remains reasonably uniform, the vortex-array model discussed earlier could be developed to include the intervortex interactions, which will capture the streamwise evolution of the vortex-array configuration. The corresponding change in gust uniformity could then be computed and used to assess the streamwise domain within which gusts with acceptable uniformity are generated. This work is underway and is outside the present scope.

On the other hand, the oscillatory component of the nonuniformity could be improved by reducing the spacing between the VGs. This would have the added benefit of increasing the gust strength by increasing the circulation per unit length of the vortex array. A limitation on reducing this spacing is the stability of the vortex array. To understand this, consider the schematic of generated vortices in Fig. 3. A vortex in the middle of the array is "induced" to move away from the top wall by its neighboring vortex on the right, which is counterbalanced by its neighbor on the left. Imperfection in the induced velocity from the two sides could cause the vortex to move in one direction or the other, which would disrupt the organization of the entire array and the uniformity of the transverse gust. Sensitivity to these imperfections increases with the reduction in the interspacing of the VGs. In our experiments, we could not maintain a stable array at spacings smaller than $0.75c_{\mathrm{VG}}$. This is reflected in the deterioration of gust uniformity as Δ_{VG} is reduced from 1.0 to $0.5c_{\mathrm{VG}}$ in Fig. 8, as discussed previously. However, we did not design the VGA to intentionally control the settings of all VGs with extreme precision. Therefore, we do believe that with the appropriate design, maintaining a stable vortex array for $\Delta_{\mathrm{VG}} < 0.75c_{\mathrm{VG}}$ could be possible, leading to improved gust uniformity and increased gust strength relative to what is reported here.

Compared to the model prediction in Fig. 6, the measured results have a lower transverse v-velocity magnitude (by ~60%). Two major sources that could be causing this discrepancy are 1) inaccuracy in the initial characteristics of the tip vortex used in the model (circulation and core radius) based on Wendt's model [16], and 2) not taking various aspects of the real flow into account in the model. These include the intervortex interactions, the viscous boundary layers on the walls, and the streamwise evolution of the vortex characteristics. The differences observed between the model and the measurements, in terms of the initial vortex size and the circulation, can be incorporated into the empirical model to further improve the model prediction. In addition, the streamwise evolution of the vortices as they interact with one another can be implemented in the model. Generally speaking, notwithstanding the quantitative difference between the experimental data and the model results, the model is a good predictor of the trends in VGA performance with changes in the various parameters of the VGA, which was the primary function of the model for the gust-generator design.

One of the key attributes of the present gust generator is that the generator does not produce turbulent fluctuations in the freestream. This feature is assessed using Fig. 11, where the RMS of both the streamwise and the transverse velocity fields are shown at steady state at the X = 650 mm measurement plane for both the baseline condition ($\alpha_{\mathrm{VG}} = 0$ deg) and with the VGA actuated to $\alpha_{\mathrm{VG}} = 16$ deg. While we do observe an increase in the fluctuation at the center of the vortices due to actuation, the central region of the test section exhibits little difference. The average fluctuation levels in the aforementioned central region ($0.4 \le \mathrm{Y/W} \le 0.6$, $0.05 \le \mathrm{Z/H} \le 0.6$) are 1.0 and 0.6% of U_∞ for u_{rms} and v_{rms}, respectively, for the baseline case, versus 1.1 and 0.6% for the actuated case.

Another significant attribute of the gust generator's design is the ability to create unsteady gusts. This is demonstrated by considering a steplike actuation from $\alpha_{\mathrm{VG}} = 0$ to 16 deg, and sinusoidal actuation $\alpha_{\mathrm{VG}} = 16 \sin 2\pi f t$ deg, with a frequency of $f = 2$ Hz. In implementation, the fidelity of the step motion is limited by the finite acceleration of the VGA hardware/drive-motor system. The actual motion profile, recorded using the servo motor's encoder, consists of an initial 2700 deg /s acceleration through the middle of the stroke, followed by a deceleration of the same magnitude as the acceleration until the end of the stroke's duration of 154 ms. The maximum nondimensional pitch rate $\Omega^* = c\alpha^*_{\mathrm{VG}}/2U_\infty$ is $\Omega^* = 0.0145$ and $\Omega^* = 0.014$ for the steplike and sinusoidal actuations, respectively. In the case of the sinusoidal actuation, this is equivalent to a reduced frequency of $k = 2\pi fc/2U_\infty = 0.05$, or a Strouhal number of $St = fA_{te}/U_\infty = 0.0066$, where A_{te} is the peak-to-peak trailing-edge amplitude.

The streamwise (u) and transverse (v) velocity components averaged over the target test region, outlined with a red broken line in Fig. 9, are shown versus time in Fig. 12 for both types of actuation. As discussed previously, the steplike actuation yields a transverse v-velocity of 5.7% of U_∞ during the actuation period; we observe here that the transverse v-velocity increases smoothly to this value with no overshoot/undershoot over a response time of ~175 ms to transition from 1 to 99% of the steady-state v value. There is a slight delay (~60 ms) from when the VGA is actuated ($t = 3$ s) to when a change in velocity is observed, but this delay is consistent with the

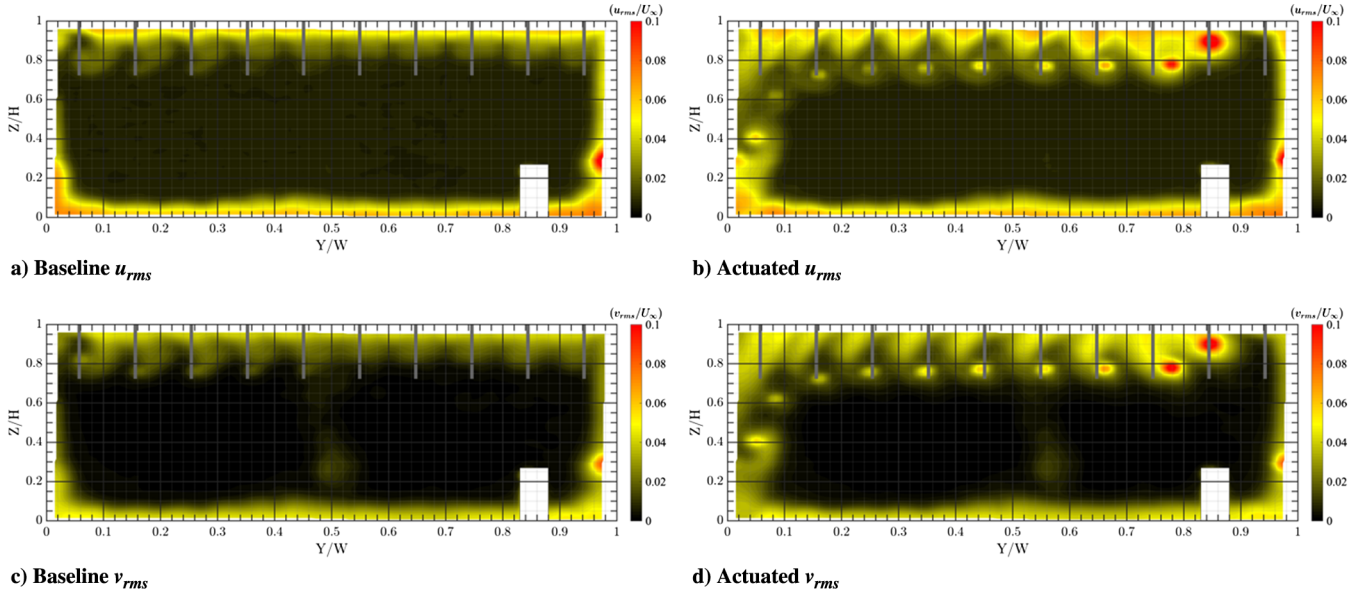

Fig. 11 Measured RMS of a–b) streamwise and c–d) transverse velocities at a downstream distance of X = 650 mm downstream of the VGA with a, c) $\alpha_{\mathrm{VG}} = 0$ deg and b,d) $\alpha_{\mathrm{VG}} = 16$ deg.

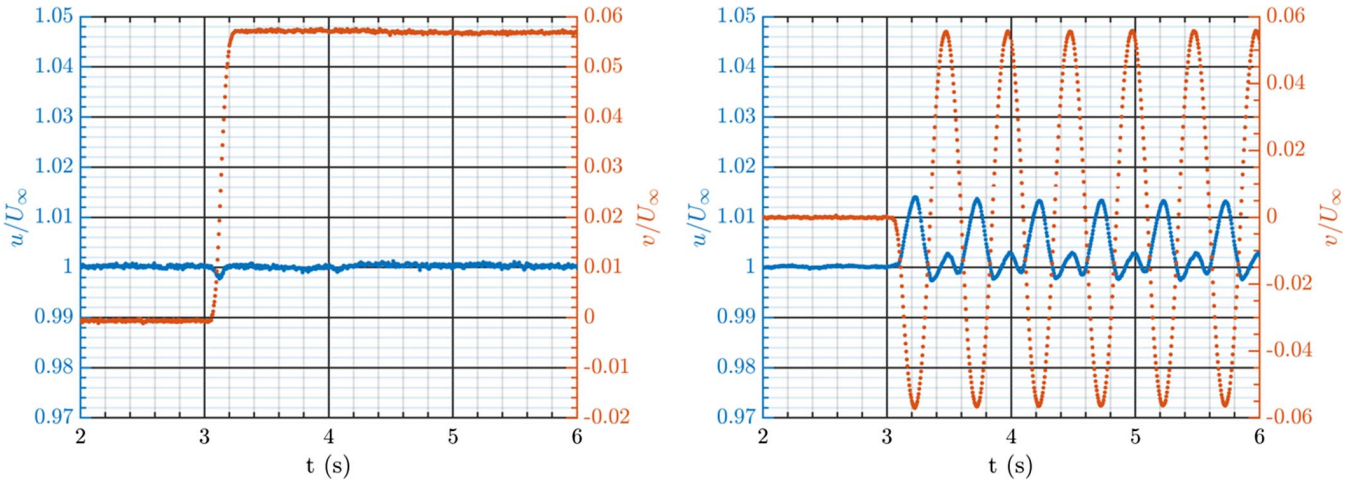

a) Steplike gust **b) Sinusoidal gust**

Fig. 12 Streamwise and transverse v-velocity components during a) steplike and b) sinusoidal actuations. Separate axis with corresponding color depicts each of the velocity components.

convective time over the distance from the VGs to the downstream measurement location at the freestream velocity.

The required response time of 175 ms for the gust to reach steady state is partly due to the inherent response dynamics of the system, and it is partly due to the fact that the steplike motion of the VGA takes 154 ms to complete. In an effort to separate both of these effects, the observed gust history is assumed to be the output of a first-order dynamical system that is excited by the steplike α_{VG} input. Following Duhamel's integral, the experimentally recorded history of α_{VG} is convolved with the theoretically known impulse response of the first-order system to obtain the expected gust response for the first-order system. For the calculation, the system's gain (fractional gust strength per unit angle of attack) is computed from the steady-state values of the angle of attack and the gust strength. The time constant is then computed via iteration until a visually good comparison is achieved between the experimentally observed and computed gust history. This comparison is shown in Fig. 13 for the time period during which the gust strength changes from the initial to the final value. As seen from the figure, for the case tested, the first-order system approximation represents the VGA response reasonably well. The analysis yields a time constant of 10 ms for the first-order system model, i.e., inherent dynamics of the gust generator.

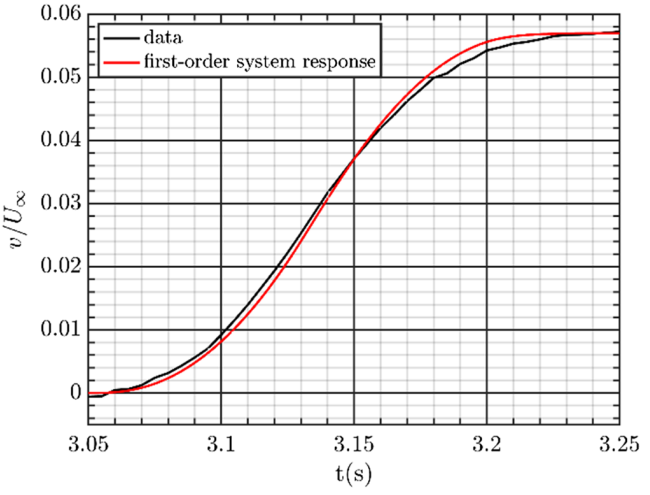

Fig. 13 Comparison between the experimentally observed and the modeled transient response of the gust generator for the steplike input.

The transverse v-velocity of the sinusoidal actuation reaches an amplitude of nearly the same magnitude as the steplike motion, with only a slight asymmetry for positive versus negative velocity (which is attributed to friction in the mechanical linkage of the VGA). The equality of the sine-wave amplitude to that of the steady-gust velocity, which implies quasi-steady operation of the VGA at 2 Hz, is consistent with the response dynamics inferred previously through the first-order system analysis. Specifically, the identified system's time constant of 10 ms corresponds to a cutoff (−3 dB) frequency of approximately 16 Hz, which is well above the 2 Hz frequency used

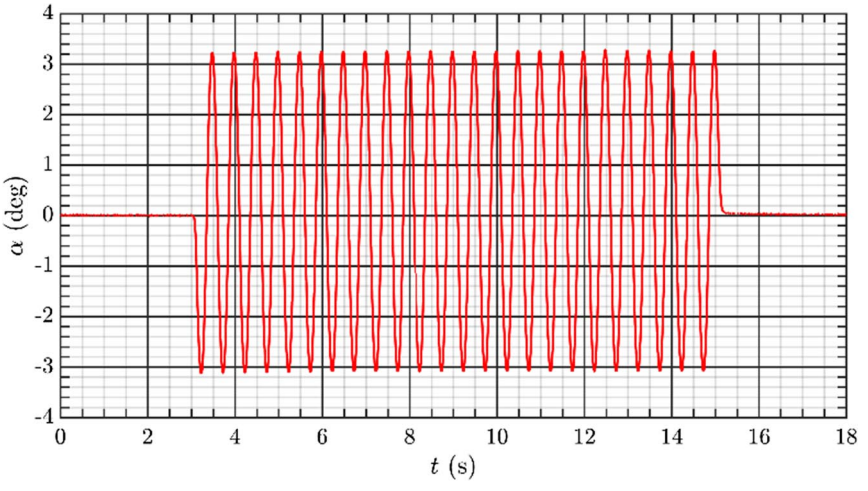

Fig. 14 Time series of the variation in the freestream's angle.

Downloaded by MICHIGAN STATE UNIVERSITY on January 21, 2021 | http://arc.aiaa.org | DOI: 10.2514/1.J059962

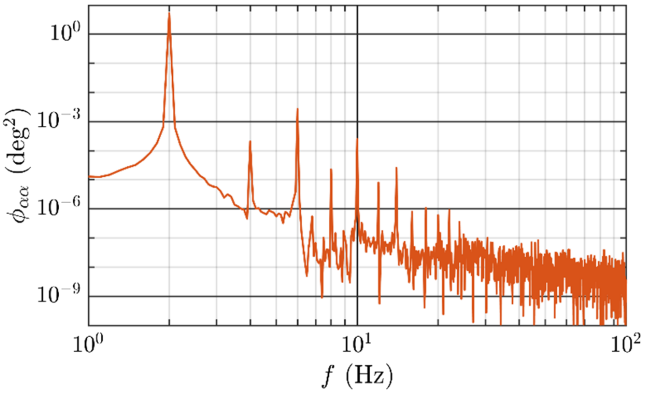

Fig. 15 Power spectrum of the unsteady portion of α time series shown in Fig. 14.

for the sinusoidal actuation. The first-order system's amplitude attenuation expected at this frequency is 0.8%, which is consistent with the experimentally observed agreement between the amplitude of the sinusoidal gust and the steady-state magnitude of the gust in the steplike actuation. Additionally, based on the first-order model, the expected phase lag at 2 Hz is 7.16 deg.

The steplike actuation shows minimal effect on the streamwise velocity, characterized by a decrease in the velocity during the actuation time by a magnitude of only $0.002U_\infty$. A different behavior is observed in the sinusoidal actuation case, with the streamwise velocity varying between $1.014U_\infty$ and $0.998U_\infty$. The asymmetry in the response is likely a peculiarity with our particular setup. While these changes in streamwise velocity are already small, they could be mitigated by incorporating a streamwise-gust louver system, placed at the downstream end of the test section, to provide the necessary "antigust."

In addition to characterizing the magnitude of the transverse gust, it is important to consider the strength of the angle-of-attack disturbance of $\alpha = \tan^{-1}(v/u)$, produced by the gust. Figure 14 shows the approach stream's angle α variation calculated from the measured $u(t)$ and $v(t)$ for the sinusoidal actuation shown in Fig. 12b. The variation has a sinusoidal shape with an amplitude of 3.25 deg. This significant swing in the freestream direction, which can be potentially doubled with the use of a second VGA on the wind tunnel's floor, is practically pure harmonic in form. This may be seen in Fig. 15, where the power spectrum of the angle variation is displayed. The spectrum shows that the dominant frequency is 2 Hz, which is the same as the pitch frequency of the VG s. The next significant peak is at 6 Hz, but it is three orders of magnitude smaller than the peak at 2 Hz. This further demonstrates that the asymmetry in the parasitic $u(t)$ component does not produce a significant harmonic distortion of $\alpha(t)$.

V. Conclusions

A novel transverse-gust generator has been modeled, designed, and tested in a wind tunnel. The gust generator consists of a vortex-generator array mounted to the wall of the wind tunnel's test section. In comparison to other approaches, the primary advantage of the new gust generator is that it can produce a transverse gust with a good degree of uniformity without increasing the turbulent fluctuations in the freestream. A simple vortex-array model is used to aid in designing a prototype of the gust generator for experimental characterization. Certain qualitative trends of the performance of the gust generator are captured well using the model. However, other aspects of the generator's behavior, as well as quantitative estimates of the gust velocity, do not agree well with experimental characterization of the generator. Further improvement of the vortex-array model to make it a useful design tool is possible by 1) incorporating additional empirical information to improve the specification of the vortex characteristics based on the geometry of the VGs, and 2) accounting for intervortex interactions and streamwise evolution of the vortex characteristics.

The gust-generator prototype is used to demonstrate the ability of the VGA to produce unsteady gusts with strength up to ±5.7% of freestream velocity within a central core region of the test section. This is accomplished for both steplike and sinusoidal gusts. The latter is used to produce oscillation in the freestream direction of ±3.25 deg at a frequency of 2 Hz and a freestream speed of 10 m/s. These variations are found to exhibit practically pure-harmonic oscillation. The spatial uniformity of the generated gust was found to be 12% of the gust velocity over 50% of the test-section height and 20% of its width, which is better than that produced by comparable methods found in the literature.

The aforementioned results are produced using one VGA along one of the tunnel walls. The use of a second VGA on the opposite tunnel wall would double the gust strength. The choice of the oscillation frequency of 2 Hz is rather arbitrary and, with appropriate choice of driving motor/motors and VGs design, it is expected that higher oscillation frequencies would be possible. Moreover, a discussion is provided in the paper on how it would be possible to further improve the gust uniformity and increase the gust strength by decreasing the interspacing of the vortex generators.

Acknowledgments

This project is funded by Office of Naval Research grant number N00014-16-1-2760. The authors would like to thank one of the reviewers for bringing to our attention the idea of using a first-order dynamical system model to represent the gust generator's response. The views and conclusions contained in this document are those of the authors and should not be interpreted as representing the official policies, either expressed or implied, of ONR or the U.S. Government. The U.S. Government is authorized to reproduce and distribute reprints for government purposes, notwithstanding any copyright notation herein.

References

[1] Perrotta, G., and Jones, A. R., "Unsteady Forcing on a Flat-Plate Wing in Large Transverse Gusts," *Experiments in Fluids*, Vol. 58, No. 8, 2017, Paper 101. https://doi.org/10.1007/s00348-017-2385-z

[2] Corkery, S. J., Babinsky, H., and Harvey, J. K., "On the Development and Early Observations from a Towing Tank-Based Transverse Wing–Gust Encounter Test Rig," *Experiments in Fluids*, Vol. 59, No. 9, 2018, Paper 135. https://doi.org/10.1007/s00348-018-2586-0

[3] Smith, Z. F., Jones, A. R., and Hrynuk, J. T., "Micro Air Vehicle Scale Gust-Wing Interaction in a Wind Tunnel," *2018 AIAA Aerospace Sciences Meeting, AIAA SciTech Forum*, AIAA Paper 2018-0573, Jan. 2018. https://doi.org/10.2514/6.2018-0573

[4] Poudel, N., Yu, M., Smith, Z. F., and Hrynuk, J. T., "A Combined Experimental and Computational Study of a Vertical Gust Generator in a Wind Tunnel," *2019 AIAA Aerospace Sciences Meeting, AIAA SciTech Forum*, AIAA Paper 2019-2166, Jan. 2019. https://doi.org/10.2514/6.2019-2166

[5] Stapountzis, H., "An Oscillating Rig for the Generation of Sinusoidal Flows," *Journal of Physics E: Scientific Instruments*, Vol. 15, No. 11, 1982, pp. 1173–1176. https://doi.org/10.1088/0022-3735/15/11/012

[6] Harding, S. F., and Bryden, I. G., "Generating Controllable Velocity Fluctuations Using Twin Oscillating Hydrofoils," *Journal of Fluid Mechanics*, Vol. 713, Dec. 2012, pp. 150–158. https://doi.org/10.1017/jfm.2012.442

[7] Brion, V., Lepage, A., Amosse, Y., Soulevant, D., Senecat, P., Abart, J. C., and Paillart, P., "Generation of Vertical Gusts in a Transonic Wind Tunnel," *Experiments in Fluids*, Vol. 56, No. 7, 2015, Paper 145. https://doi.org/10.1007/s00348-015-2016-5

[8] Ham, N. D., Bauer, P. H., and Lawrence, T. L., "Wind Tunnel Generation of Sinusoidal Lateral and Longitudinal Gusts by Circulation Control of Twin Parallel Airfoils," NASA CR 137547, 1974.

[9] Tang, D. M., Cizmas, P. G. A., and Dowell, E. H., "Experiments and Analysis for a Gust Generator in a Wind Tunnel," *Journal of Aircraft*, Vol. 33, No. 1, 1996, pp. 139–148. https://doi.org/10.2514/3.46914

[10] Gilman, J., Jr., and Bennett, R. M., "A Wind-Tunnel Technique for Measuring Frequency-Response Functions for Gust Load Analyses," *Journal of Aircraft*, Vol. 3, No. 6, 1966, pp. 535–540. https://doi.org/10.2514/3.43773

Downloaded by MICHIGAN STATE UNIVERSITY on January 21, 2021 | http://arc.aiaa.org | DOI: 10.2514/1.J059962

[11] Giuni, M., and Green, R. B., "Vortex Formation on Squared and Rounded Tip," *Aerospace Science and Technology*, Vol. 29, No. 1, 2013, pp. 191–199.
https://doi.org/10.1016/j.ast.2013.03.004

[12] Naguib, A. M., Vitek, J., and Koochesfahani, M. M., "Finite-Core Vortex Array Model of the Wake of a Periodically Pitching Airfoil," *AIAA Journal*, Vol. 49, No. 7, 2011, pp. 1542–1550.
https://doi.org/10.2514/1.J050881

[13] Wendt, B. J., Reichert, B. A., and Foster, J. D., "The Decay of Longitudinal Vortices Shed from Airfoil Vortex Generators," *13th AIAA Applied Aerodynamics Conference*, AIAA Paper 1995-1797, June 1995.

[14] Wendt, B. J., and Reichert, B. A., "The Modeling of Symmetric Airfoil Vortex Generators," *34th Aerospace Sciences Meeting*, AIAA Paper 1996-0807, Jan. 1996.
https://doi.org/10.2514/6.1996-807

[15] Wendt, B. J., and Reichert, B. A., "Spanwise Spacing Effects on the Initial Structure and Decay of Axial Vortex Generators," NASA CR 198544, Nov. 1996.

[16] Wendt, B. J., "Initial Circulation and Peak Vorticity Behavior of Vortices Shed from Airfoil Vortex Generators," NASA CR 2001-211144, Aug. 2001.

[17] Wendt, B. J., "Parametric Study of Vortices Shed from Airfoil Vortex Generators," *AIAA Journal*, Vol. 42, No. 11, 2004, pp. 2185–2195.
https://doi.org/10.2514/1.3672

[18] Hamedani, B. A., Naguib, A. M., and Koochesfahani, M. M., "Reynolds Number Effect on Lift Characteristics of an Airfoil Translating Across a Non-Uniform Approach Flow," *2019 AIAA Aerospace Sciences Meeting, AIAA SciTech Forum*, AIAA Paper 2019-0639, Jan. 2019.
https://doi.org/10.2514/6.2019-0639

[19] Hultmark, M., and Smits, A. J., "Temperature Corrections for Constant Temperature and Constant Current Hot-Wire Anemometers," *Measurement Science and Technology*, Vol. 21, No. 10, 2010, Paper 105404.
https://doi.org/10.1088/0957-0233/21/10/105404

A. R. Jones
Associate Editor

Downloaded by MICHIGAN STATE UNIVERSITY on January 21, 2021 | http://arc.aiaa.org | DOI: 10.2514/1.J059962